

# **Evaluation of Fiber Distribution and Alignment in Structural UHPC Elements**

## **Authors and Affiliation:**

Elizabeth (Nadelman) Wagner, Wiss, Janney, Elstner Associates, Inc., enadelman@wje.com  
John S. Lawler, Wiss, Janney, Elstner Associates, Inc.

## **Abstract:**

The high tensile strength and excellent post-cracking ductility of ultra-high performance concrete (UHPC) makes it attractive for structural applications. This desirable behavior derives in part from a dense network of fibers - often made of high strength steel - that carry tensile loads, even after the concrete has cracked. The orientation and spatial arrangement of the fibers has a significant impact on the ability of the UHPC to carry these stresses. However, because UHPC is typically placed as a highly flowable material, the fibers have a tendency to align along the direction of flow and may also segregate through the depth of the element, thereby altering the local mechanical properties of the UHPC within the structural element. This paper presents a brief review of fiber distribution and alignment in UHPC composites and the associated impact on the performance of structural UHPC elements. An image analysis technique is described to characterize distribution and alignment of fibers on a cut surface, after the exposed fiber surfaces were highlighted by treatment with a copper sulfate solution. A "fiber alignment factor" is introduced to relate the flexural performance of sawed beams to fiber distribution and alignment. Fiber alignment parameters are compared to the theoretical parameters obtained for a random (isotropic) distribution of fibers to characterize the influence of preferential alignment on the mechanical response of the UHPC beams. Extension of the image analysis technique to characterizing fiber distribution and alignment in field-cast structural elements is also discussed.

**Keywords:** UHPC, fiber alignment, image analysis, flexural testing, fiber distribution

## **1. Introduction**

The high tensile strength and excellent post-cracking ductility of ultra-high performance concrete (UHPC) makes it an attractive option for structural applications. Although the tensile capacity of conventional concrete is typically not sufficient to be utilized in structural design, the use of steel fiber reinforcement in UHPC enhances the material's tensile performance to the extent that it can be relied upon in the design of structural elements. When steel fibers are present in sufficient quantity and well-distributed throughout the UHPC matrix, the material will exhibit strain-hardening behavior, to a peak post-cracking direct tensile strength of 1 ksi (7 MPa) or more (Russell and Graybeal 2013). Strain-hardening of UHPC and other fiber-reinforced concrete composites is characterized by a continued increase in the tensile capacity, even after cracking has initiated. This behavior is possible because a portion of the tensile load is carried by the fibers. Efficient fiber bridging across cracks causes multiple cracks to form without sudden failure of the element, and because of the often exceptionally high tensile strength of the steel fibers and the excellent bond of the UHPC to the fibers, this effect leads to the characteristic high post-cracking ductility exhibited by UHPC (Naaman 2017).

For UHPC to exhibit high tensile capacity and post-cracking ductility, the fibers must be well-distributed throughout the element's cross-section and oriented such that they can be engaged under tensile loading. Fibers oriented perpendicular to a tensile stress will provide little benefit to the composite in terms of tensile performance and ductility. Studies have shown that the distribution and alignment of fibers within a UHPC element strongly depend on the manner in which the element is produced (Kang et al. 2011; Wille and Parra-Montesinos 2012; Maya, de la Varga, and Graybeal 2016; Walsh et al. 2018). In particular, fibers will tend to align along the direction of flow through forms (Wille and Parra-Montesinos 2012; Maya, de la Varga, and Graybeal 2016), and consequently, the placement methods and formwork geometry will have a pronounced effect on the orientation and distribution of fibers within a structural UHPC element. In addition, highly flowable UHPC may be susceptible to fiber segregation (Graybeal 2014), which can further alter the distribution of fibers within a structural element, and consequently, its performance under tensile loads.

As UHPC is increasingly used in structural applications worldwide, simple characterization methods are needed for understanding the impact of placement methods and material flow on fiber distribution and alignment and thus the mechanical performance of UHPC. This paper presents a simple image analysis technique that may be used to characterize fiber distribution and alignment in cores or sections cut from UHPC elements, and introduces a "fiber alignment factor", which quantifies the average impact of fiber orientation and distribution on the tensile performance of a UHPC element. Further extensions of the image analysis technique to assess the spatial distribution of fibers within an element (e.g., due to fiber segregation or restricted flow), to quantify variations in fiber alignment around joints or other features, or to troubleshoot the cause of low strength in field- or laboratory-cast UHPC, are also discussed.

## **2. Mathematical Framework**

A straight steel fiber used to enhance the tensile performance of UHPC may be approximated mathematically by a right circular cylinder. When a right circular cylinder is intersected by a plane, it creates an ellipse on the surface of that plane, as shown in Figure 1. The ellipse is characterized by a major and minor axis of lengths  $a$  and  $b$ , which are related to the geometry of the fiber and the angle that the fiber intersects the plane. Specifically, the length of the minor axis ( $a$ ) is equal

to the diameter of the fiber, while the ratio of the minor axis to the major axis ( $a/b$ ) is equal to the sine of the angle ( $\theta$ ) that the fiber makes with a vector perpendicular to the intersecting plane.

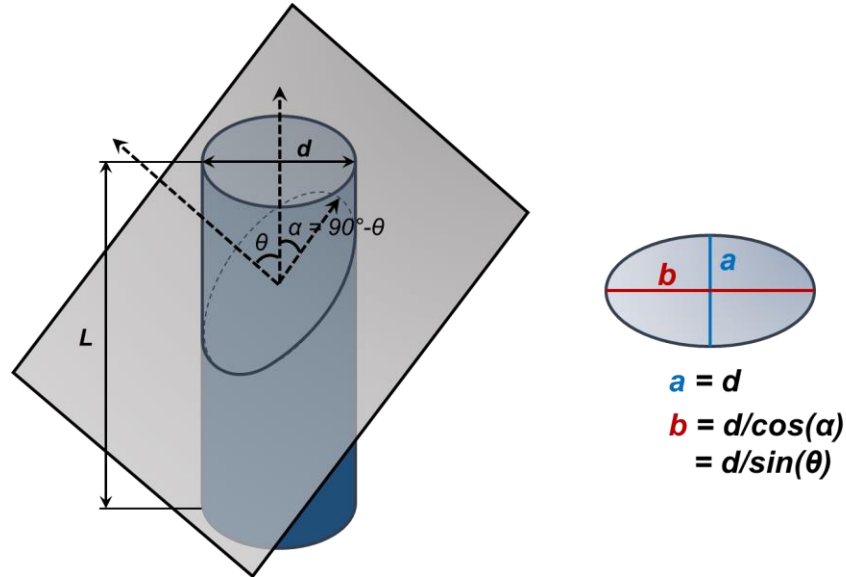


**Figure 1. Schematic illustration of an ellipse formed by a plane intersecting a cylinder.**

Based on these simple mathematical principles, it is possible to determine the orientation angle of any fiber in three-dimensional space simply by knowing the lengths of the major and minor axes of the ellipse formed by the fiber and a cutting plane. It is therefore possible to use basic image analysis techniques to quantify the spatial distribution and orientation of fibers on a cut surface of a core or beam cut from a structural UHPC element (Wang et al. 2017; Tiberti et al. 2018; Huang et al. 2018) and relate those parameters to the tensile response of the element.

### 3. Experimental and Analytical Methods

#### 3.1 Specimen Fabrication

Six beams, nominally 4-inches by 4-inches by 14-inches (100 mm by 100 mm by 350 mm) were cut from a flat, 10-foot by 10-foot by 4-inch (305 cm by 305 cm by 10 cm) panel element, cast using a UHPC mixture with a w/cm of 0.17, a compressive strength of 18 ksi (124 MPa), and containing 2 percent straight steel fibers by volume. The fibers had a tensile strength of 400 ksi (2750 MPa), a nominal width of 0.008 in (0.2 mm), and an aspect ratio of 65.

The UHPC was transported from the batch plant to the panel form using a forklift-mounted bucket. The material was placed into the form at a single location near the center of one edge, causing the material to flow across the length of the panel to the other side. The material initially flowed easily out of the bucket into the form with a flow spread of 10 inches (250 mm) when measured according to ASTM C1856, but quickly lost workability as the concrete underwent early-age drying in the hot ambient temperature (90 °F / 32 °C) and light breeze at the placement location. The rapid loss of workability limited the lateral flow distance of the UHPC, such that shoveling was required to fill the extreme corners of the panel form, as shown in Figure 2.

After the panel was stripped from its form, the six beams were removed by saw-cutting (ASTM C42) from a location approximately 1 foot (30 cm) from the edge of the panel opposite the point of placement, as marked in Figure 2. Three beams (A, B, and C) were cut with their

longitudinal axis parallel to the primary direction of flow, and three beams (D, E, and F) were cut with their longitudinal axis perpendicular to the primary direction of flow. The beams were further trimmed in the laboratory by running the cut faces along the edge of a wet saw until the surfaces were square with the formed (bottom) and finished (top) surfaces of each beam.



**Figure 2. Filling of panel forms with UHPC. Approximate locations of cut flexural beam specimens are shown. Arrow indicates direction of UHPC flow.**

### ***3.2 Flexural Performance***

Flexural testing was performed for each beam under third-point bending, essentially according to ASTM C1609. A 12-inch (30 cm) span length was used for all six beams. The beams were tested under displacement control to a mid-span deflection of  $L/150$ , or 0.08 inches (2 mm). The test deviated from ASTM C1609 only in that the beams were tested in a dry condition (not saturated), and the formed (bottom) surface of each beam was loaded in tension.

### ***3.3 Image Analysis***

After flexural testing had been completed, a slice was cut across the full cross-section of each beam, immediately adjacent the widest crack that formed. The face of the slice closest to the crack was polished by lapping with successively finer abrasives until the surface was smooth and contained no visual saw-cuts or grooves. To enhance the visual contrast between the steel fibers and the surrounding UHPC mortar, the polished surfaces of each slice were treated with a copper sulfate solution, which plated the steel with copper and slightly lightened the surrounding paste. Each polished and plated cross-section was imaged in 48-bit color using a flat-bed scanner at 1200 dpi resolution. At this resolution, the fiber diameter of 0.008 inches (0.2 mm) is 9 pixels.

The scanned images were cropped so that the analyzed image contained only the full cross-section of each specimen, with no background, then processed using a MATLAB script developed to identify each fiber within the cross-section and to characterize its alignment. The MATLAB program consisted of the following steps:

1. Read the image.
2. Use L\*a\*b\* color space thresholding to separate the copper-colored fibers from the predominantly gray background image.
3. Convert the thresholded image to a binary (black-and-white) image, with fibers represented by white pixels (value 1) and the background represented by black pixels (value 0).
4. Identify each fiber in the image. Remove noise by excluding any features that contain fewer pixels than the smallest nominal fiber area (70 pixels).
5. Calculate the area fraction of fibers in the image as the percentage of white pixels in the processed and filtered image.
6. Fit an ellipse to each fiber detected. Exclude any features that have a minor axis length smaller than the width of one fiber (9 pixels) or larger than the width of two fibers (19 pixels).
7. Using the properties of the fitted ellipses, calculate the orientation of each fiber relative to the longitudinal axis of the beam. A fiber with an orientation angle of  $0^\circ$  is aligned along the longitudinal axis of the beam, and a fiber with an orientation angle of  $90^\circ$  lies perfectly flat against the cut surface.

An example 0.5-inch (13 mm) square segment of one of the images analyzed is shown in Figure 3. Note that in Figure 3c, a bundle of fibers near the center of the image was excluded from the angle analysis based on length of the bundle's minor axis. Excluded fiber bundles typically accounted for less than 1 percent of all fibers detected in each image.

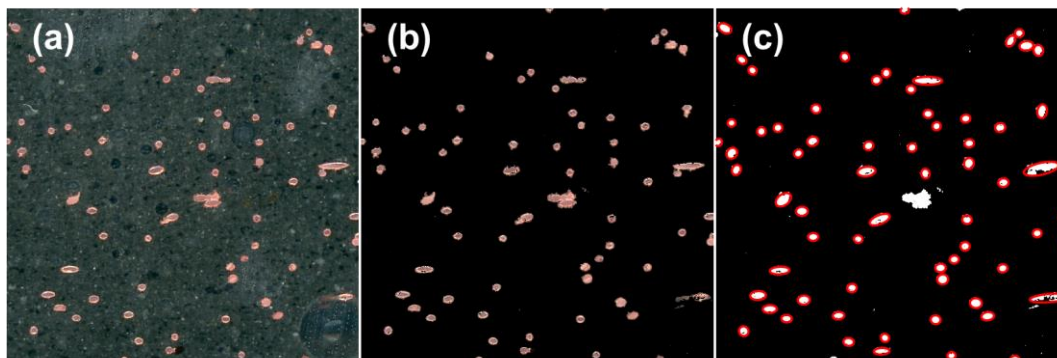


**Figure 3. (a) Segment of original scanned image showing fibers in copper and paste in gray. (b) Color-thresholded image separating the fibers from the paste background. (c) Binary image with ellipses (red) fitted around fibers (white) included in the analysis.**

## 4. Results

### 4.1 Flexural Performance

The flexural performance of each beam was characterized in terms of its first-crack (first-peak) flexural strength and peak flexural strength. The results are presented in Table 1. On average, beams cut with their longitudinal axis parallel to the primary direction of flow had greater first-crack and peak flexural strengths than beams cut with their longitudinal axis perpendicular to the flow. The highest flexural strength was observed for Beam A, which was cut parallel to the direction of flow, and the lowest flexural strength was observed for Beam E, which was cut perpendicular to the direction of flow.

**Table 1. Flexural Strength of Beams and Fiber Density of Cut Cross-Sections**

Beam	A	B	C	D	E	F
Cut Type	I	I	I	II	II	II
First-Crack Flexural Strength (psi)	1,610	1,290	1,220	960	670	820
Peak Flexural Strength (psi)	2,590	1,850	1,220	1,300	760	1,120
Fiber Density (fibers per in <sup>2</sup> )	206	157	156	88	120	122
Fiber Area Fraction (%)	3.6	2.0	2.3	2.1	2.7	2.4
Fibers Aligned 0 to 45° (%)	73.8	62.7	65.7	34.5	39.5	51.8

Notes: Cut Type I = Longitudinal axis of beam parallel to primary direction of flow

Cut Type II = Longitudinal axis of beam perpendicular to primary direction of flow

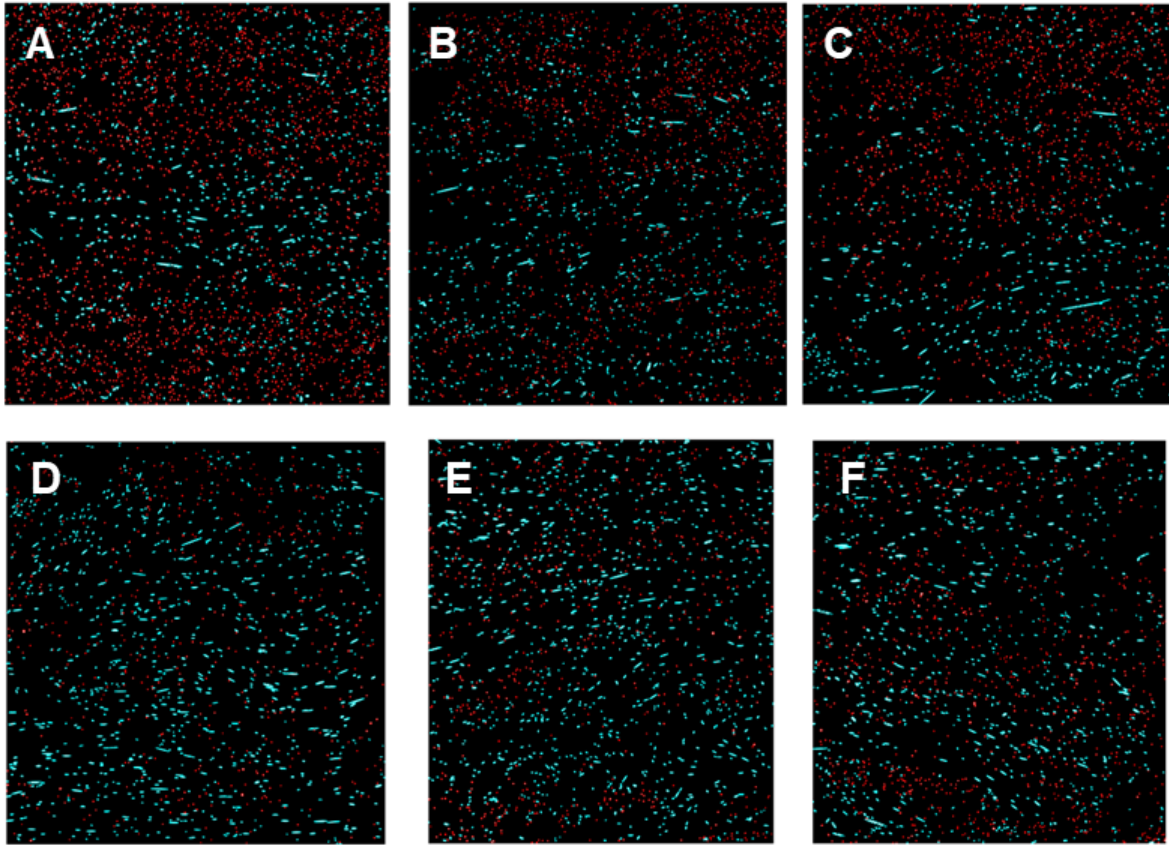
145 psi = 1 MPa; 1 in<sup>2</sup> = 6.45 cm<sup>2</sup>

#### 4.2 Image Analysis

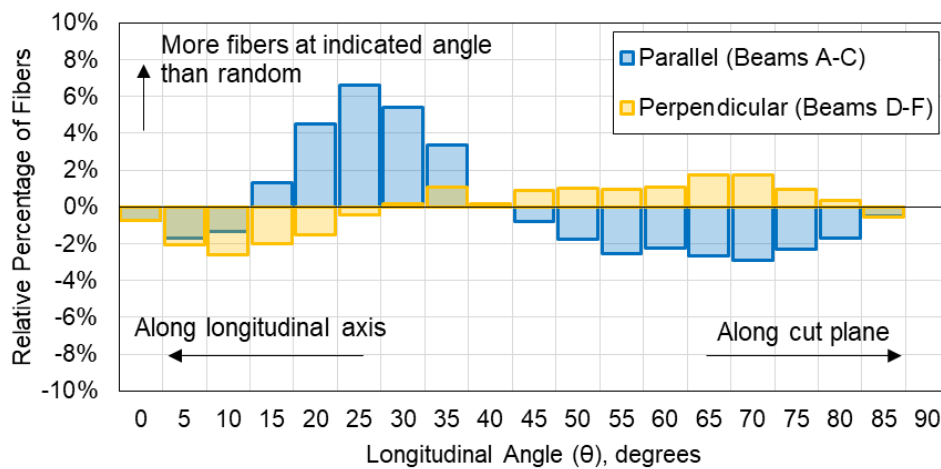
The area fraction and density of fibers in each cross-section, as determined by image analysis, are summarized in Table 1. The fiber area fractions ranged between 2.0 and 3.6 percent, with most beams having fiber contents near the 2.0 percent anticipated by the mix design. (Note: Fiber area fraction is an estimator for fiber volume fraction.) The fiber densities ranged between 88 and 206 fibers per square inch (14 and 32 fibers per cm<sup>2</sup>), with Beams A, B, and C, having a 57 percent greater average fiber density (173 fibers per in<sup>2</sup>; 27 fibers per cm<sup>2</sup>) than Beams D, E, and F (110 fibers per in<sup>2</sup>; 17 fibers per cm<sup>2</sup>). The measured fiber density is related, in part, to the orientation of the fibers relative to the cutting plane; fibers oriented along the longitudinal axis of these beam are more likely to intersect the cutting plane. These longitudinally-oriented fibers also have a more direct impact on flexural performance, therefore, it is not surprising that Beam A, which had the greatest fiber density, also had the greatest flexural strength of the six beams evaluated.

Figure 4 shows a visual representation of the fiber alignment for all six cross-sections. Fibers with preferential alignment (oriented mostly along the longitudinal axis of the beam, at an angle,  $\theta$ , of 45° or less) are shown in red, while fibers with less preferential alignment (i.e., at an angle greater than 45°) are shown in blue. It can be seen from the figure that a larger percentage of the fibers in Beams A, B, and C are aligned along the longitudinal axis of the beam than in Beams D, E, and F, which is consistent with the greater flexural performance exhibited by these beams. In addition, it can be seen that Beam A has a large number of preferentially-aligned fibers distributed over its entire cross section, while the preferentially-aligned fibers in Beams B and C are primarily localized in the top half of the beams. The clustering of preferentially-aligned fibers in the top half of the cross-section provides limited benefit to the flexural resistance at the bottom face of the beam, where the tensile stresses are greatest. Thus, based on differences in the spatial distributions of the preferentially-aligned fibers, it is not surprising that the flexural strengths of Beams B and C were lower than that of Beam A.

The fiber orientations for each beam segment were also compared to the theoretical fiber orientations for a random (i.e., isotropic) arrangement of fibers. The theoretical percentage of fibers at each longitudinal angle,  $\theta$ , in a random arrangement is equal to  $2\sin(\theta)\cos(\theta)$ . Figure 5 shows the average percentage of fibers measured at each angle for the two groups of beams, relative to the theoretical percentage of fibers at that angle for a random fiber arrangement. A positive relative percentage indicates that more fibers are aligned along a particular direction than would be expected for a random arrangement. The results show that the fibers in the beams cut parallel to the direction of primary flow have a greater-than-random tendency to be aligned along the longitudinal axis of the beam, while the fibers in the beams cut perpendicular to the direction of primary flow have a greater-than-random tendency to be aligned parallel to the cut plane.



**Figure 4. Spatial distribution of aligned fibers for Beams A-F. Fibers shown in red have a longitudinal alignment angle between  $0^\circ$  and  $45^\circ$  (aligned primarily along longitudinal axis), and fibers shown in blue have a longitudinal angle between  $45^\circ$  and  $90^\circ$  (aligned primarily along cut surface). Cut surface in Beams A, B, and C is perpendicular to UHPC flow direction; cut surface in Beams D, E, and F is parallel to UHPC flow direction.**



**Figure 5. Average percentage of fibers at each alignment angle, relative to the expected percentage for a “random” distribution of fibers. (Legend shows orientation of axis of beam relative to UHPC flow direction.)**

## 5. Correlations to Flexural Performance

As previously described, the high tensile strength of the steel fibers will contribute to the tensile capacity of a UHPC element, provided that the fibers are aligned along the direction of principal tension. The image analysis and flexural strength results suggest that the greater-than-random tendency for fibers to align along the longitudinal axis of Beams A, B, and C contributed to the improved flexural performance of those beams relative to Beams D, E, and F, which showed a less-than-random tendency to align favorably. To further quantify this effect, two parameters were considered: an “average axial alignment factor”,  $\bar{k}_\theta$ , and a “fiber alignment factor,”  $f$ .

The average axial alignment factor,  $\bar{k}_\theta$ , is a dimensionless parameter associated with the tensile contribution of each fiber perpendicular to the cut plane. This factor is calculated according to Equation 1:

$$\bar{k}_\theta = \sum_{i=1}^{N_f} \cos(\theta_i) / N_f \quad (1)$$

where  $\theta_i$  is the longitudinal angle of each fiber  $i$  and  $N_f$  is the total number of fibers in the cross section. Essentially,  $\bar{k}_\theta$  is the average of the cosine of each angle,  $\theta$ , for every fiber in the cross-section (Figure 6). A beam with fibers aligned all along the longitudinal axis ( $\theta = 0^\circ$ ) will have  $\bar{k}_\theta = 1$ , a beam with fibers aligned all along the cut surface ( $\theta = 90^\circ$ ) will have  $\bar{k}_\theta = 0$ , and a beam with fibers aligned at random will have  $\bar{k}_\theta = 2/3$ .

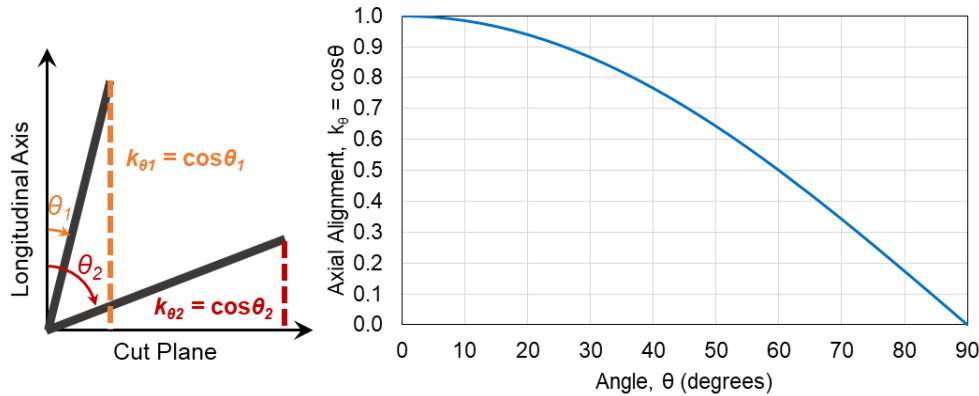


**Figure 6. Axial alignment as a function of longitudinal angle  $\theta$  of an individual fiber.**

The fiber alignment factor,  $f$ , is a dimensioned parameter that quantifies the total contribution of the fibers in a unit area to the tensile capacity of the UHPC perpendicular to the cut plane. It can be computed according to Equation 2:

$$f = N_f \bar{k}_\theta / A \quad (2)$$

where  $A$  is the area of the cross section. The fiber alignment factor,  $f$ , combines both characterization of the fiber alignment with characterization of the fiber density.

The  $\bar{k}_\theta$  and  $f$  parameters calculated for each beam are summarized in Table 2. The values of  $\bar{k}_\theta$  for all three parallel-cut beams (A, B, and C) were greater than  $\bar{k}_\theta$  for a random arrangement of fibers, indicating more preferential alignment of the fibers in these beams, on average. Likewise, the value of  $f$  for Beams A, B, and C (averaging 130 per in<sup>2</sup>, 20 per cm<sup>2</sup>) was nearly double that of Beams D, E, and F (averaging 69 per in<sup>2</sup>, 11 per cm<sup>2</sup>), indicating a greater potential contribution of the fibers to the flexural-tensile performance of the beams. A moderate correlation was found between the fiber alignment factor  $f$  and the first-peak and peak flexural strengths of the beams (Figure 7), further supporting the notion that flexural performance is related to both the distribution and the alignment of the fibers within the beam’s cross-section. However, the correlation is limited

in that flexural performance is also a function of the bond characteristics of the UHPC matrix and the mechanical performance of the matrix itself, which are not directly considered by this factor.

**Table 2. Alignment Factors for Cut Cross-Sections**

Beam	A	B	C	D	E	F
Average Axial Alignment, $k_\theta$	0.775	0.727	0.742	0.577	0.618	0.673
Fiber Alignment Factor, $f$ (1/in <sup>2</sup> )	160	114	116	51	74	82

Notes:  $k_\theta$  for a random arrangement of fibers = 0.667.  
 1 in<sup>2</sup> = 6.45 cm<sup>2</sup>

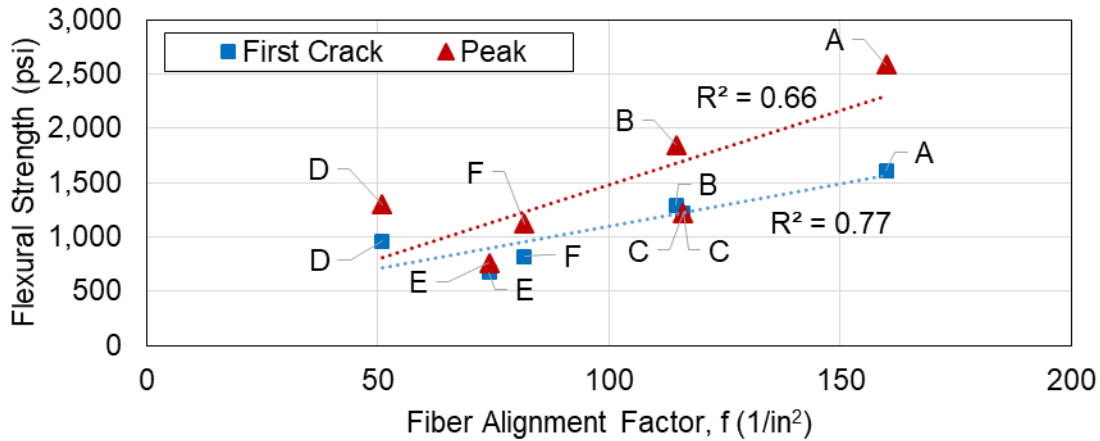


**Figure 7. First-crack and peak flexural strength versus fiber alignment factor  $f$ .**

## 6. Conclusions

This paper presented a simple, image analysis-based method for characterizing fiber distribution and alignment on cut UHPC surfaces after the fibers were highlighted by treatment with a copper sulfate solution. The primary benefit of this technique is its ability to provide insight into the flexural and tensile performance of a UHPC element without the need for sophisticated laboratory equipment. Key findings of this study include the following:

- Image analysis can effectively characterize the tendency for fiber alignment for various placement methods. In this case, beams cut with their longitudinal axis parallel to the direction of UHPC flow exhibited more favorable alignment than would be expected for a random arrangement of fibers, while beams cut with their longitudinal axis perpendicular to the direction of flow exhibited less favorable alignment than for a random arrangement of fibers.
- Fiber alignment and distribution are both important for the flexural performance of UHPC elements. Beams with well-aligned but poorly dispersed fibers (e.g., Beams B and C) exhibited reduced flexural performance compared to beams with well-aligned and well-distributed fibers (e.g., Beam A).
- Local tensile performance can be correlated to the fiber alignment factor  $f$ , which considers both fiber density and alignment. For the six beams evaluated,  $f$  was found to correlate to both first-crack and peak flexural strengths.
- The image analysis methods presented may be extended for use in other evaluations of UHPC elements, including characterization of fiber alignment in flexure-critical or shear-critical sections of structural mock-ups, quantification of fiber segregation in elements with deep cross-sections or cast using highly flowable UHPC, or troubleshooting low strength results in field- or laboratory-cast UHPC.

## **7. References**

- Graybeal, B., “Design and Construction of Field-Cast UHPC Connections,” FHWA, U.S. Department of Transportation, Report No. FHWA-HRT-14-084, 2014.
- Huang, H., Gao, X., Li, L. and Wang, H., “Improvement Effect of Steel Fiber Orientation Control on Mechanical Performance of UHPC,” *Construction and Building Materials*, Vol. 188, November 2018, pp. 709-721.
- Kang, S.T., Lee, B.Y., Kim, J.-K., and Kim, Y.Y., “The Effect of Fibre Distribution Characteristics on the Flexural Strength of Steel Fibre-Reinforced Ultra High Strength Concrete,” *Construction and Building Materials*, Vol. 25, No. 5, May 2011, pp. 2450-2457.
- Maya, L.F., de la Varga, I., Graybeal, B.A., “Fiber Reinforcement Influence on the Tensile Response of UHPFRC,” *Proceedings of the First International Interactive Symposium on UHPC*, Des Moines, Iowa, July 18-20, 2016.
- Naaman, A. E., *Fiber Reinforced Cement and Concrete Composites*. Sarasota, Florida: Techno Press 3000, 2017.
- Russell, H.G. and Graybeal, B.A., “Ultra-High Performance Concrete: A State-of-the-Art Report for the Bridge Community,” FHWA, U.S. Department of Transportation, Report No. FHWA-HRT-13-060, 2013.
- Standard Test Method for Flexural Performance of Fiber-Reinforced Concrete (Using Beam with Third-Point Loading), ASTM C1609 / C1609M-12, ASTM International, West Conshohocken, PA, 2012, www.astm.org.
- Standard Test Method for Obtaining and Testing Drilled Cores and Sawed Beams of Concrete, ASTM C42 / C42M-18, ASTM International, West Conshohocken, PA, 2018, www.astm.org.
- Tiberti, G., Germano, F., Mudadu, A., and Plizzari, G.A., “An Overview of the Flexural Post-Cracking Behavior of Steel Fiber Reinforced Concrete,” *Structural Concrete*, Vol. 19, 2018, pp. 695-718.
- Walsh, K.K., Hicks, N.J., Steinberg, E.P., Hussein, H.H., and Semendary, A.A., “Fiber Orientation in Ultra-High-Performance Concrete Shear Keys of Adjacent-Box-Beam Bridges,” *ACI Materials Journal*, Vol. 115, No. 2, March 2018, pp. 227-238.
- Wang, R., Gao, X., Huang, H., and Han, G., “Influence of Rheological Properties of Cement Mortar on Steel Fiber Distribution in UHPC,” *Construction and Building Materials*, Vol. 144, July 2017, pp. 65-73.
- Wille, K. and Parra-Montesinos, G.J., “Effect of Beam Size, Casting Method, and Support Conditions on Flexural Behavior of Ultra-High-Performance Fiber-Reinforced Concrete,” *ACI Materials Journal*, Vol. 109, No. 3, May 2012, pp. 379-388.

## **8. Acknowledgements**

The authors would like to acknowledge Mason Lampton, Kurt Podoll, and the staff at Standard Concrete Products in Tampa, Florida, for producing and obtaining the beam specimens evaluated in this paper. We would also like to thank Mark Haddad, Daniela Mauro, and Alan Stone at WJE for their assistance in the laboratory with specimen preparation, testing, and imaging.